Nano Energy 62 (2019) 513–520

Contents lists available at ScienceDirect

Nano Energy

journal homepage: www.elsevier.com/locate/nanoen

Communication

Enhanced photocatalytic H_2 evolution by plasmonic and piezotronic effects based on periodic Al/$BaTiO_3$ heterostructures

Limin Guo[a,b,c], Caifu Zhong[d], Jinqing Cao[a,b], Yanan Hao[a], Ming Lei[a], Ke Bi[a,*], Qijun Sun[b,c,**], Zhong Lin Wang[b,c,e,***]

[a] State Key Laboratory of Information Photonics and Optical Communications, School of Science, Beijing University of Posts and Telecommunications, Beijing, 100876, China
[b] Beijing Institute of Nanoenergy and Nanosystems, Chinese Academy of Sciences, Beijing, 100083, China
[c] School of Nanoscience and Technology, University of Chinese Academy of Sciences, Beijing, 100049, China
[d] Chinese Academy of Macroeconomic Research, National Development and Reform Commission, Beijing, 100038, China
[e] School of Materials Science and Engineering, Georgia Institute of Technology, Atlanta, GA 30332-0245, United States

ARTICLE INFO

Keywords:
Al/$BaTiO_3$ heterostructure
Plasmonic photocatalysis
Piezotronic effect
H_2 evolution
Localized surface plasmon resonance

ABSTRACT

Plasmonic catalysis of solar water splitting has been extensively exploited these years for the fast-growing energy demands and environmental friendliness. However, most of the plasmonic systems are restricted on the noble metals and semiconductors, which limited the cost efficiency of the photocatalysts and further investigations of metal plasmons coupling with other research filed. Herein, we presented nonprecious Al@$BaTiO_3$ (Al/BTO) plasmonic heterostructures on Ti foams for a synergistic piezo-photocatalytic water splitting and pollutant degradation. An impressive local surface plasmon resonance (LSPR) and solar energy harvesting ability (in the ultraviolet–visible light region) are achieved on the Al/BTO photoelectrode, which endow the heterostructure with an excellent solar H_2 evolution (327 μmol h^{-1} cm^{-2}) and 4-nitrophenol (4-NP) degradation rate. Furthermore, the BTO substrates upon magnetic field induced mechanical stimuli provide a strong polarization potential to the plasmonic catalyst by significantly enhancing the photo-generated carrier separation and transfer. The synergistic piezo-photocatalysis exhibited almost 50% increase in the H_2 production (657 μmol h^{-1} cm^{-2}) and decolourization of 4-NP, which is comparable to a traditional noble metallic plasmonic photoelectrode. The hybrid catalyst delivers a long-term durability in the cycling tests, maintaining ~90% of the activity after 30 h. This work demonstrates that non-noble metallic plasmons and piezoelectronic effect can serve synchronously as highly active photocatalytic agents, which not only boost the solar energy conversion efficiency but also decrease the material cost.

1. Introduction

As a “green chemistry” approach, hydrogen (H_2) generation by means of solar water splitting has been extensively exploited to satisfy the fast-growing energy demands in an environmental friendliness fashion [1,2]. Photocatalytic water splitting, a commonly used catalysis process, utilizes wide bandgap semiconductors (*e.g.* TiO_2, ZnO, $SrTiO_3$, et al.) to initiate a water redox reaction by the photo-generated electrons (or holes) [3–6]. However, the wide bandgap semiconductors only responding to the UV light (< 10% in solar light) severely limits the photocatalytic efficiency regardless of the rapid recombination of the excited electrons and holes in the homogeneous semiconductor catalysts [7,8]. Recently, plasmonic nanomaterials have gained intensive attention in the research fields of spectroscopic sensors and solar energy conversion due to the excellent photocatalytic performance. The plasmonic catalysts are ready to strongly interact with the incident light through the excitation of a localized surface plasmon resonance (LSPR), exhibiting a tunable absorbance in the visible light (vis-light) or near-infrared light (NIR-light) range [2]. Generally, LSPR often relies on the noble metals (*e.g.* gold (Au), silver (Ag), and platinum (Pt)) [9–11] with high surface charge carrier concentration, which is readily to cause a natural resonance with incident light [12]. To overcome the obstacles of low resource reserves and high cost, non-noble metals, metal oxides, metal chalcogenides and metal nitrides

* Corresponding author.
** Corresponding author. Beijing Institute of Nanoenergy and Nanosystems, Chinese Academy of Sciences, Beijing, 100083, China.
*** Corresponding author. Beijing Institute of Nanoenergy and Nanosystems, Chinese Academy of Sciences, Beijing, 100083, China.
E-mail addresses: bike@bupt.edu.cn (K. Bi), sunqijun@binn.cas.cn (Q. Sun), zhong.wang@mse.gatech.edu (Z.L. Wang).

https://doi.org/10.1016/j.nanoen.2019.05.067
Received 30 April 2019; Received in revised form 23 May 2019; Accepted 27 May 2019
Available online 30 May 2019

have recently been extensively exploited for the plasmonic photocatalysis [13–16]. Aluminum (Al), an earth-abundant and tractable material, has attracted significant attentions from scientists [17]. Al catalyst provides the plasmonic resonance in a broad spectrum from UV to NIR region, which is highly desirable for plasmon-enhanced solar energy conversion and catalysis. Al is also a very stable photocatalyst due to the formation of the self-protecting native oxide layer on metal surface that prevents the continuous oxidation by photocorrosion [16]. The optical properties of Al are well described in the literatures that a UV-dipole plasmon peak usually appears on Al nanoparticles because of their more negative dielectric constant compared with silver and gold [18]. According to the Drude-Lorentz model involving the dielectric function and resonant frequency of Al plasmons, [2] high tunability of the LSPR from UV to visible light can be achieved by the hybridization of Al nanoparticles with high dielectric constant materials, such as perovskite or oxide materials ($BaTiO_3$, $SrTiO_3$, TiO_2, et al.).

$BaTiO_3$ (BTO) is a classic piezoelectric and ferroelectric oxide material, which can create an inner piezoelectric potential under mechanical force according to the crystal deformation (especially the noncentrosymmetric tetragonal phase) [19,20]. When the piezopotenital is coupled with semiconducting properties or photoexcitation (*i.e.* piezoelectric semiconductor, such as ZnO, GaN, InAs, and MoS_2), [21–24] it can readily modulate the transport or generation/separation/recombination of the charge carriers across the M-S contact or p-n junction, [25–27] which is classified in piezotronics and piezophototronics [28–33]. The induced piezoelectric polarization by mechanical strain is also promising for influencing various photocatalytic reactions, such as water splitting, [16] photoelectrochemical polymerization, [34] degradation of organic pollutants, [35] et al. (referred as piezo-photocatalysis in this work) [36]. As the most widely used piezoelectric material, the nano-scaled BTO materials usually have oxygen defects on the surface, in which the excess electrons act as the dopants and affect the energy band structure of BTO, leading to partial semiconducting properties [5]. When the energy band edge of BTO nanomaterials is located within the near UV light region, photocatalytic activity even under the solar light irradiation has been demonstrated. Hence, the piezoelectric BTO with partial semiconducting properties hybridized with efficient plasmonic catalysts may lead to significantly enhanced photocatalysis process according to the piezo-photocatalysis effect.

In this work, we design BTO nanocavity arrays loaded with periodically distributed Al nanoparticles on flexible Ti foam for plasmonic solar water splitting and photo-degradation of organic pollution (4-nitrophenol, 4-NP). The heterostructured photocatalyst represents greatly improved photocatalysis performance on H_2 evolution and organic pollution degradation under magnet vibration where the piezoelectric material suffers from mechanical external force and generate piezoelectric polarization to the photocatalyst, *i.e.* piezotronic effect enhanced plasmonic photocatalysis. The BTO nanocavity arrays functionalize as an ideal dielectric shell for Al plasmons. Moreover, its polarization plays an important role in the photocatalytic process by further assisting the separation of photo-generated electron-hole pairs due to the built-in piezoelectric field. The morphology, element compositions, surface chemical states and photochemical activities of the heterostructures are investigated in details. The H_2 release efficiency based on the piezo-photocatalyst is enhanced by more than 50% at a reproducible rate of 657 $\mu mol\, h^{-1}\, cm^{-2}$ compared with the pristine photocatalyst. The degradation rate of organic pollutes is also enhanced by ~100%. The proposed piezo-photocatalysts is prospective to be employed for highly efficient, cost-effective, large-scale, and long-term utilization for H_2 evolution and environment protection.

2. Results and discussion

The preparation processing of the Al/BTO photocatalysts is illustrated in Fig. 1a. Firstly, periodic honeycomb-shaped TiO_2 nanocavity arrays (NCAs) are directly made on the surface of the Ti foams by anodic oxidation. Then, a hydrothermal reaction is carried out for the TiO_2 NCAs in a Teflon-lined stainless-steel autoclave filled with 70% of 0.001 M $Ba(OH)_2$ solution (180 °C, 3 h). In the final step, 10 nm Al is deposited on the BTO/Ti hybrid foams by an e-beam evaporator and constructs into an Al/BTO/Ti plasmonic heterostructure after the dewetting process. The morphology of the heterostructures is displayed in Fig. 2 and Fig. S1. The pristine anodized TiO_2 nanocavities have an average pore size of 50 nm and wall thickness of ~10 nm (Fig. 2a, **a1**). It is notable that the BTO nanocavities obtained by hydrothermal method exhibit an obvious wall thickening (from 10 to 20 nm) due to the crystal cell expansion during the reaction (Fig. 2b, **b1**) [37]. After a rapid heat treatment at 350 °C for 1 h in N_2 flow, the deposited Al is converted into Al nanoparticles (average particle size is ~40 nm), which distribute periodically into the BTO NCAs (Fig. 2c, **c1**). At the beginning of the thermal dewetting, continuous Al layer is divided into discontinuous patches owing to pinning effect of BTO substrate and the flowability of Al. These small patches form detached islands inside BTO nanocavities and further agglomerate to form discrete Al nanoparticles in the cooling down step. These discrete Al NPs, with a diameter of ~40 nm, individually half-fill the BTO nanocavities and attach mostly at the top side of inner wall. The cross-section of the Al/BTO heterostructures are revealed in Figs. S1e and S1f. The transmission electron microscopy (TEM) images show a highly-ordered lamination of the Al cores and BTO shells in the heterostructure. The high-resolution TEM image in Fig. 2d1 demonstrates two different crystal structural domains, which are assigned to the Al particle and BTO wall, respectively. The inside domain exhibits a fringe spacing of ca. 0.236 nm (Fig. 2d1), corresponding to the (111) planes of Al [38]. The energy dispersive X-ray spectrometry (EDS) mapping of the Al/BTO heterostructure clearly shows the immobilized Al cores in the BTO nanocavities, forming a seamless connection at the interface (Fig. 2e). The individual elements of Ba, Ti and Al are assembled uniformly at the corresponding locations.

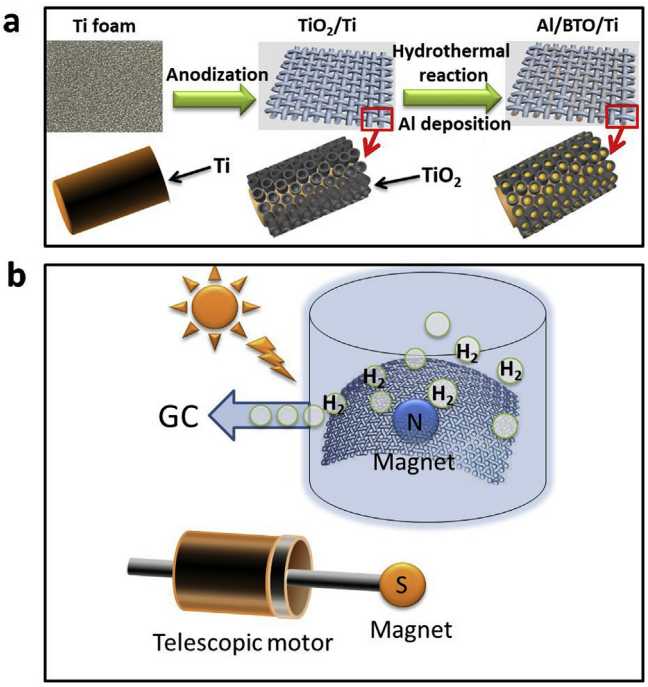

Fig. 1. (a) Synthesis process of the TiO_2 NCAs, BTO NCAs and Al/BTO heterostructures on Ti foam. (b) Schematic illumination of the application of Al/BTO/Ti heterostructure toward solar water splitting by the assistance of magnetic vibration motor.

X-ray diffraction (XRD) patterns of the heterostructures are revealed in Fig. 3a. The pattern of the directly anodized sample (TiO_2/Ti) is mainly indexed to the Ti substrate (PDF file No. 44–1294). The weak

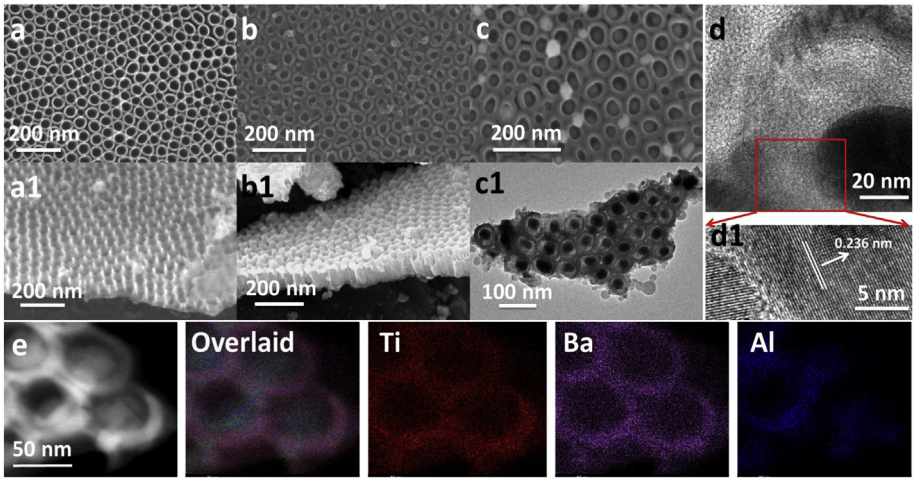

Fig. 2. SEM images of the (a, a1) TiO_2, (b, b1) BTO and (c) Al/BTO NCAs. (c1, d, d1) TEM and HRTEM images of the Al/BTO heterostructure. (e) STEM image and the corresponding EDS elemental mapping of Bi, Ti and Al in Al/BTO, respectively.

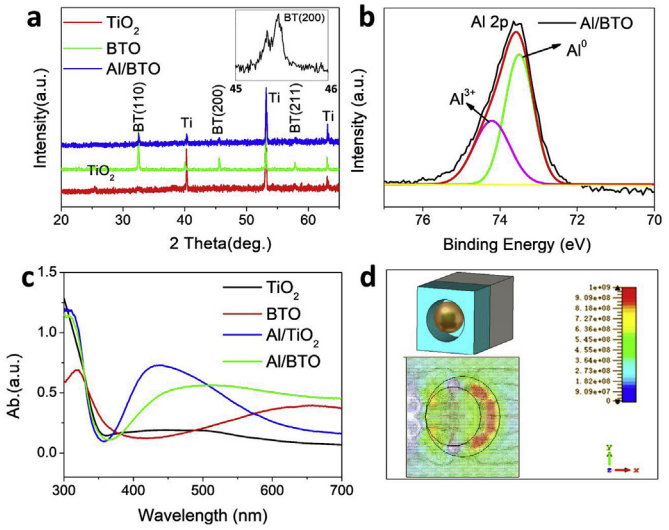

Fig. 3. (a) XRD patterns of TiO_2, BTO and Al/BTO NCAs on the Ti foam. (b) High-resolution XPS spectrum of Al (Al 2p peak) in the Al/BTO with the fitted binding energy belonging to the diverse chemical states. (c) UV–vis absorption spectra when using TiO_2, BTO, Al/TiO_2 and AL/BTO NCAs as photoelectrode, respectively. (d) FEM simulation of Al/BTO for a function of electromagnetic field distribution.

peak at 25.3° can be assigned to anatase TiO_2 (PDF file No.21–1272). After the hydrothermal treatment in 0.001 M $Ba(OH)_2$ aqueous solution, the anodic TiO_2 nanocavities are transformed to tetragonal $BaTiO_3$ (PDF file No. 75–1606) with an apparent peak splitting at 45.4°. After assembling the Al nanoparticles into the BTO nanocavities by physical precipitation and dewetting treatment, the XRD pattern remains the same with that of BTO/Ti, indicating small loading amount of Al nanoparticles in the heterostructures. X-ray photoelectron spectroscopy (XPS, Fig. S2 and Fig. 3b) demonstrates the composition and surface chemical state of the samples at different steps. Ti 2p spectra are detected in all samples with the high-resolution spectral peaks centered at 463.7 eV and 457.9 eV (Fig. S2b, indexed to Ti $2p_{1/2}$ and Ti $2p_{3/2}$ in the lattice matrix of TiO_2 or BTO). The Ba 3d spectrum is detected in the BTO/Ti and Al/BTO/Ti heterostructures, further confirming the transformation of the TiO_2 NCAs to BTO NCAs during the hydrothermal reaction (Fig. S2c). The Al 2p spectrum is found after the e-beam deposition and thermal dewetting process with two fitted peaks at 74.2 eV and 73.5 eV, which is attributed to the trivalent Al in Al_2O_3 (74.2 eV) and ground state metallic Al (73.5 eV), respectively (Fig. 3b and Fig. S2a). The atomic ratio of Al_2O_3 integrated from the peak area is ca. 30%, suggesting a slight surface oxidization of the Al nanoparticles.

To estimate the potential photochemical catalysis feasibility of the as-prepared samples, the optical response in the UV–vis light region is measured and shown in Fig. 3c. Apart from the intrinsic absorption of TiO_2 and BTO at the wavelength less than 370 nm (band gap of sole TiO_2 and BTO is approximately 3.3 eV), [3,36] Al nanoparticles exhibit clear LSPR behavior with the peaks centered at 450 nm and 500 nm for Al/TiO_2 and Al/BTO, respectively. The red-shift and broadening of the plasmonic resonance peak in Al/BTO is a direct consequence of the larger dielectric constant of BTO compared with TiO_2, which can be understood through equation (1) [17]:

$$\omega_{SPR} \approx \frac{\omega_P}{\sqrt{1 + 2\varepsilon_m}} \quad (1)$$

where ω_p is the absorption frequency of the bulk metal (ω_p of Al is 3.57×10^{15} Hz, always in UV range), ω_{SPR} is the frequency of LSPR, and ε_m is dielectric constant of the medium materials outside Al. The red-shift of the resonant wavelength occurs when the dielectric constant of the medium or nanoparticle size of the Al increases. The weak absorption peak of sole BTO NCAs (Fig. 3c) at the red-light region (650–700 nm) may be ascribed to the photonic band-gap that usually happens in the periodic perovskite materials [5]. To elucidate the electromagnetic field enhancement in the Al/BTO plasmonic structure and potential active sites during photocatalysis, the finite element method simulation (FEM, COMSOL 5.2) is introduced for the Al/BTO NCAs. Owing to the LSPR effect, a highly concentrated plasmonic hot spot is found at the edge of the Al particle with a thickness of 3–5 nm (cross-section view at the *x*-*y* plane, Fig. 3d) by use of the polarized light at the wavelength of 500 nm (the incident light illuminates from the top of the BTO NAC along the *z*-axis). The enhanced electromagnetic fields are estimated as the key factors to excite the electron-hole separation and increase the solar energy conversion efficiency during photocatalysis process [39].

The solar water splitting performance is investigated by utilizing the TiO_2, BTO, Al/TiO_2 and Al/BTO NCAs as photoelectrodes, respectively. The whole reaction process is monitored by a gas chromatograph. The H_2 evolutions of all the samples show linear increment trends according to the catalysis time (5 h) under solar light irradiation (Fig. 4a). It can be found that the pure TiO_2 or BTO NCAs show a limited H_2 evolution rate because of their limited photo-response in the solar spectra. It is notable that the BTO substrates are endowed with semiconducting property due to the naturally formed surface defects during the hydrothermally synthesis and [5,19]. These defects are essential for

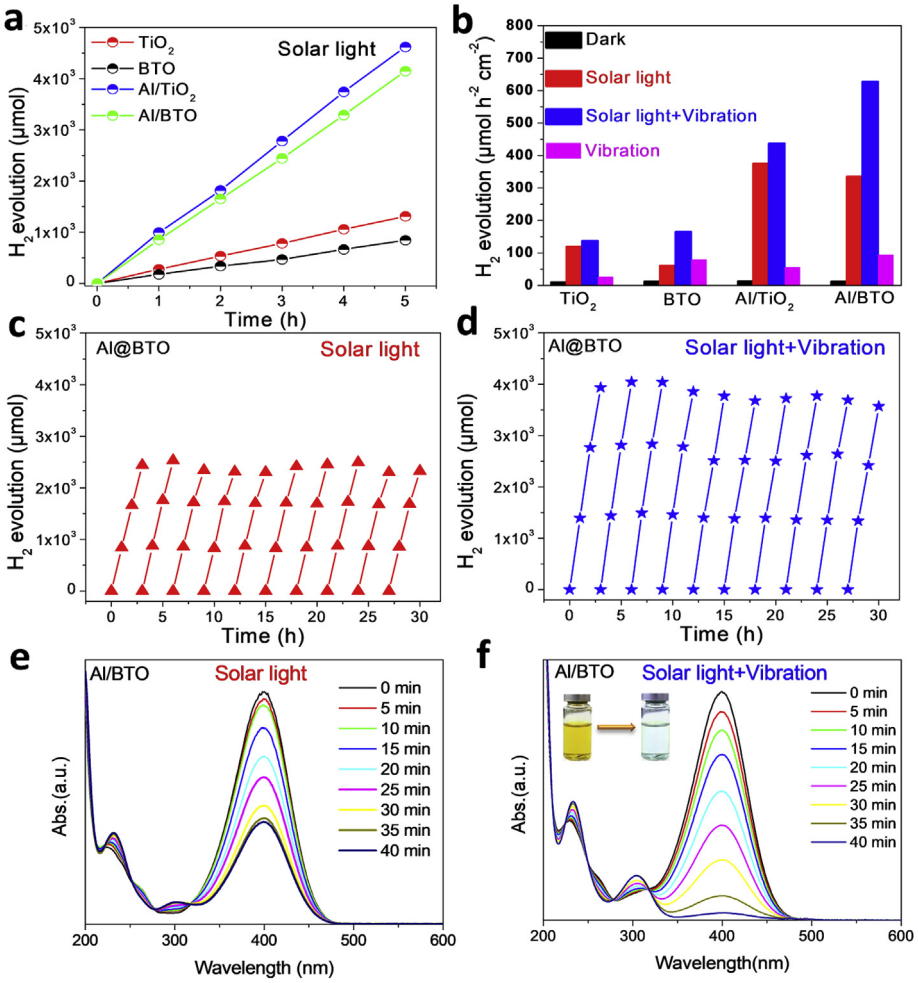

Fig. 4. (a) Time-dependent photocatalytic H_2 evolution of different samples and (b) average H_2 yield rate as the functions of different excitation mode. (c, d) Recycling performance of Al/BTO heterostructure in 30 h of continuous reaction upon the solar light irradiation as well as both solar light and magnetic vibration. (e, f) Time dependent absorption spectra for the photocatalytic and piezo-photocatalytic reduction of 4-NP by $NaBH_4$ in presence of Al/BTO.

assisting photoelectrons transfer. Among the different catalysts, the Al decorated samples (both Al/TiO_2 and Al/BTO) exhibit a much higher H_2 release efficiency than that of the TiO_2 or BTO NCAs without Al precipitation. The results indicate that the hybridization of Al nanoparticles with semiconducting substrates can induce an enhanced LSPR activity. The normalized photocatalytic H_2 yield rates according to the geometric area of the samples are shown in Fig. 4b (the mass production of H_2 by the weight of the catalyst is provided in Fig. S3a). In the dark condition, all the samples show almost no catalytic capacity with negligible amount of evolved gas ($< 15\,\mu mol\,h^{-1}\,cm^{-2}$). In contrast, the solar-light-driving gas release rate is drastically increased to 105, 48, 362 and 327 $\mu mol\,h^{-1}\,cm^{-2}$ for TiO_2, BTO, Al/TiO_2 and Al/BTO samples, respectively. The superior solar energy conversion rate for H_2 evolution based on the Al/TiO_2 heterostructures may be attributed to the higher conductivity of TiO_2 substrate than that of BTO. Photogenerated electrons are easily transferred to the conductive band of TiO_2 and then delivered to the active sites on the surface [40]. Electrochemical impedance spectroscopic (EIS) and time-dependent photocurrent density are employed to provide further insight into the charge-transfer kinetics in the samples under simulated solar light illumination (Fig. S3c, **S3d**). The pure TiO_2 substrate exhibits a lower charge-transfer resistance than that of BTO owing to the better conducting nature. Moreover, TiO_2 is identified to have a stronger photocurrent density than that of BTO. It is notable that the charge-transfer ability of the catalysts after Al deposition is further enhanced, representing superior catalytic activity upon LSPR. Interestingly, when a magnetically intermittent vibration is introduced to the photoelectrode, the H_2 release amount based on the Al/BTO heterostructures is substantially enhanced by more than 50% to a reproducible rate of 657 $\mu mol\,h^{-1}\,cm^{-2}$, which is comparable to the some noble metal plasmonic catalysts (Table S1). Control experiments performed only under magnetic field induced vibration present a much lower activity than the photocatalytic or the synergistic piezo-photocatalytic process. This result delivers two important revelations: (i) the LSPR effect of the heterostructures is a crucial factor to initiate the solar water splitting performance; (ii) the piezoelectric effect of BTO substrate plays a complementary and significant role to further enhance the catalysis efficiency after the photocatalytic process is initiated.

To further evaluate the piezotronic effect on the plasmonic photocatalysis performance induced by LSPR, surface photovoltage spectroscopy (SPV) is employed to investigate the induced photovoltages of the polarized and unpolarized Al/BTO photoelectrode under light irradiation. The polarization process of the BTO substrate is conducted by an atomic force microscope (AFM) under a bias voltage of −1 V in the piezoresponse force microscopy (PFM) mode. As shown in Fig. S3, the response spectrums of Al/TiO_2 and Al/BTO heterostructures are higher than that of the pure BTO (in the visible light region), indicating photogenerated electron-hole pairs on the surface of the photocatalytic heterostructures according to the LSPR of Al plasmons. The polarized Al/BTO heterostructures show the highest surface photovoltage (with wavelength from 500 to 525 nm), indicating more active behaviors of the photo-generated electron-hole pairs due to the existent polarization

charges. This result is consistent with the photocatalytic performance of different samples toward H_2 generation. The plasmonic effect is essential to initiate the formation of electron-hole pairs to photolyze water. The piezoelectric polarization of BTO under magnetic field induced vibration plays an auxiliary and important role in the photocatalytic process by further assisting the separation of photo-generated electron-hole pairs due to the built-in electric field. To study the stability and reusability of the heterostructures, ten consecutive cycling tests are carried out among both the photocatalytic and synergistically piezo-photocatalytic conditions (Al/BTO NCAs, Fig. 4c and d). The activity of the catalyst shows negligible fading (< 10%) after 30 h, suggesting that these catalysts can prospectively be employed for long-term utilization.

The hydrogenation of organic pollutants by the assistance of a catalyst is a typical degradation process used in the environmental protection industry. The reaction of 4-NP and $NaBH_4$ (to form 4-aminophenol) is a feasible thermodynamic process, which is usually kinetically restricted in absence of catalyst. Noble metal nanoparticles are promising as the ideal catalysts for this degradation reaction, but suffering from high cost and non-recyclable utilization [41,42]. Here, Al/TiO_2 and Al/BTO NCAs are also substantiated for 4-NP reduction in presence of $NaBH_4$. As indicated in Fig. 4e, f and Fig. S4, significant decreases of the absorbance at 400 nm (characteristic band of 4-NP) are observed under solar light illumination, revealing a successful plasmonic reduction by the Al/TiO_2 and Al/BTO heterostructures with loaded Al nanoparticles. The color of the pristine solution changes from dark yellow to bright yellow in 40 min and the degradation rate (defined as C/C_0, where C is the immediate concentration and C_0 is the initial concentration of 4-NP calibrated by the absorbance at 400 nm) is calculated to be 40%–50% according to the linear fitting degree of C/C_0 versus time (Fig. S5). It is notable that the photocatalytic efficiency of Al/BTO is a little higher than that of Al/TiO_2, which may be attributed to that a tiny piezoelectric effect is induced in the Al/BTO heterostructure by a gentle stirring process during the photocatalytic reaction (to keep the uniformity of the dye solution). When the mechanical force and light irradiation are applied together to the Al/BTO catalyst, the degradation rate is enhanced by ~100% in 40 min with a complete discoloration of the yellow solution (Fig. 4e). The hybrid piezo-photocatalytic efficiency of Al/BTO is about two times higher than the single photocatalytic activity of Al/TiO_2 and Al/BTO. This result is also consistent with the above results observed during the solar water splitting. Hence, the piezo-photocatalysis is of great significance in assisting the plasmonic redox reaction by enhancing the photon-to-electron conversion efficiency and strong electron-hole separation [14,23]. The stability of the piezo-photocatalyst is also investigated by reusing it for five cycles. Almost 90% of the photocatalysis activity is maintained without obvious catalyst poisoning or deactivation, proving that the heterostructure is a relatively stable catalyst.

Fig. 5 depicts the mechanism of charge carriers generation and transfer on the Al/BTO photoelectrode during the piezo-photocatalytic process. The synergistic effect of the built-in electric field in BTO and light scattering of Al nanoparticles is suggested to explain the piezo-photocatalysis. On one hand, the defective semiconducting BTO can be partially excited by the UV-light in the solar spectrum and originate a small amount of electron-hole pairs. The hybridization of Al plasmons in BTO nanostructures can help to reduce the reflection loss according to the light scattering and promote the effective absorbance of UV-light by the Al/BTO photoelectrode. On the other hand, when the semiconducting BTO (with oxygen defects) directly contacts with the Al nanoparticles, the electrons and holes redistribute at the interface and reach an equilibrium state, where band bending happens in the BTO side (Fig. 5a). This band bending is considered as a space-charge region with a field direction indicating from BTO to Al. In the plasmonic photocatalytic process, this equilibrium energy state is broken up. The work function (E_w) of the metal particle is reduced by the LSPR, leading to the photo-generated electrons transferring to the BTO side with holes

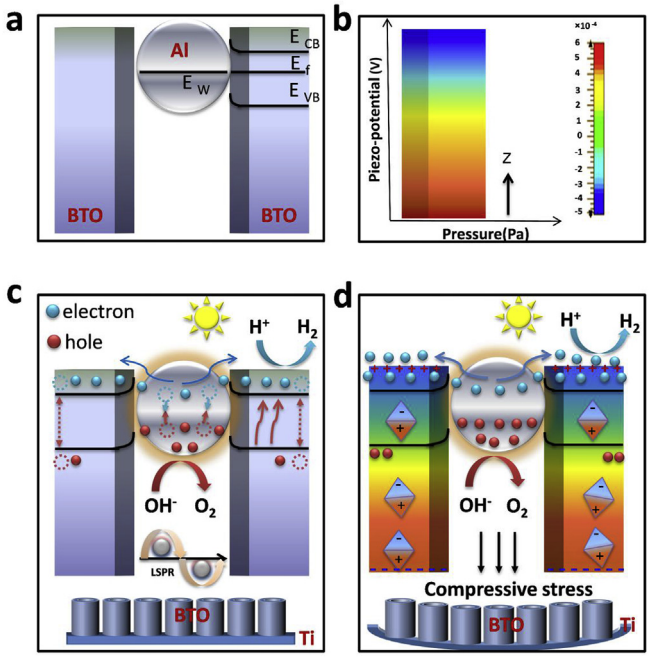

Fig. 5. The working mechanism of the plasmonic photocatalysis and piezo-photocatalysis process. (a) The natural junction Al/BTO NCA. (b) the theoretical simulation of the piezoelectric potential as a function of the mechanical stress on the BTO crystal. (c) The photocatalyic process for H_2 generation under solar light irradiation. (d) The piezo-photocatalysis process of the Al/BTO heterojunction under a polarization direction of the BTO from bottom to the top of the nanocavity.

being left (Fig. 5c). All the aforementioned electrons and holes are supposed to be separated and captured by the redox groups (the methanol and H^+) for water splitting. However, the recombination of the charge carriers is ineluctable to invalidate the catalysis reaction (dotted circles in Fig. 5c), even though the light scattering of Al nanoparticles and naturally formed space-charge region at the Al/BTO interface can partially suppress the recombination. Consequently, magnetic field is applied to the BTO substrate in this work to introduce mechanical vibration (with a compressive strain at the top side of BTO NCAs) to induce a substantial piezopotential in BTO (built-in piezopotential). Fig. 5b shows the calculated piezopotential profile of BTO by FEM under a pressure of 10^7 Pa. Under the external strains, the dispersed electric domains in BTO rotate to a similar direction and form an amplified electric field (polarization charges and surface enriched charges are assembled at both ends of BTO crystal). This built-in piezopotential has the similar electric field direction with the space-charge region, which can further boost the separation of the electron-hole pairs and optimize the redox process (Fig. 5d). Therefore, the piezo-photocatalysis is a synergistic process that involves the plasmonic, piezotronic and semiconducting properties of the hybrid catalysts. Every component (*e.g.* BTO, Al, light irradiation, and mechanical force) is essential in the highly efficient solar water splitting and pollutant degradation.

3. Conclusion

In summary, an Al/BTO piezo-photocatalyst with highly ordered nanocavity structures is designed on Ti foam. The Al/BTO heterostructures exhibit excellent photocatalytic activity, which is a synergistic combination of the piezoelectric polarization of BTO and plasmonic activities of Al nanoparticles (*i.e.* piezotronic effect enhanced photocatalysis). Under mechanical vibration and solar light irradiation, an optimized H_2 evolution rate of 657 μmol h^{-1} cm^{-2} and 4-NP degradation activity (100% degradation in 40 min) are achieved based on

the Al/BTO piezo-photocatalysts, which is more active than the sole photocatalysis process (by 50%–60%). After the cycling test for both H_2 evolution and 4-NP degradation in 30 h, the catalysts maintain ~90% of the initial piezo-photocatalysis activity, ascribed to the stable periodic BTO nanopores and immobilized Al plasmons. These heterostructures provide a new piezo-photocatalytic strategy toward industrial applications by designing proper heterostructures based on highly ordered piezoelectric materials and nonprecious plasmonic metals.

4. Experimental section

4.1. Preparation of Al/$BaTiO_3$/Ti heterostructures

Clean Titanium foams (25.4 × 25.4 × 2 mm, 99.7% purity, Kejing Corporation) were anodized by a two-electrode system in 3 M HF/H_3PO_4 (98%, Alfa, China) at 80 °C for 4 h. After anodization, the TiO_2/Ti foams were rinsed with ethanol and dried in the air. After annealing at 400 °C for 1 h, the samples were held in the center of Teflon reaction vessels. A hydrothermal solution (0.001 M barium hydroxide and 0.01 M KOH) was prepared by deionized water and filled to 70% of the vessels. Then the vessels were placed into an oven heated at 180 °C for 3 h. Finally, the samples were removed out, rinsed in deionized water and dried. An e-Beam evaporator (Kurt J. Lesker PVD75 Proline) was used to deposit Al layers onto the $BaTiO_3$/Ti (BTO/Ti) foams with a total thickness of 10 nm. Then, the as-prepared Al/BTO/Ti samples were put in a quartz-tube furnace. Thermal dewetting was carried out at 350 °C in N_2 flowing for 1 h to form Al nanoparticles.

4.2. Morphological and structural characterization

Morphologies of the anodized TiO_2 and Al/$BaTiO_3$ heterostructures were observed with a field-emission scanning electron microscope (SEM, FEI Nova NanoSEM 450) and a transmission electron microscope (TEM, FEI Tecnai G2 F30). X-ray diffraction (XRD) was obtained using an X'pert Powder (PANalytical, equipped with a Panalytical X'celerator detector using Cu Kα radiation, λ = 1.54056 Å). The chemical composition and valance state of samples were characterized by X-ray photoelectron spectroscopy (XPS, ESCALab250, Thermo VG). All high-resolution spectra were analyzed with the XPSPEAKS software. UV–vis–NIR absorption spectra were measured using a UV-3600 (SHIMADZU, Japan) spectrometer.

4.3. Photocatalytic H_2 evolution

The photocatalytic H_2 production was performed in a sealed quartz reactor (50 ml). Al/BTO/Ti foams with a size 25.4 × 10 mm (the weight of the sample is about 0.2 g cm^{-2}) were submerged in 20 ml of a mixed solution made of DI water and methanol (8:2 by volume). The samples were deformed to an arciform shape and fixed in the quartz reactor. A small magnet was tied at the top position of the arciform sample. A telescopic motor with another magnet was placed under the quartz reactor and could approach the quartz reactor intermittently. According to the magnetic force between the two magnets, a periodic vibration was achieved for Al/BTO/Ti foam. For the comparison experiments, the reactor was illuminated only by a solar light simulator (AM 1.5, 300 W Xe lamp, 100 mW cm^{-2}) or under both solar light illumination and magnet field. The gas produced from the upper space above the solution in the quartz reactor was periodically analyzed by the gas chromatograph. The electrochemical impendence spectroscopy (EIS) was collected in 1 M Na_2SO_4 aqueous solution on a CHI-760e electrochemical station. The amplitude of the alternating voltage was 5 mV, and the frequency range was from 10 mHz to 100 kHz. The time-dependent photocurrent density (in 1 M NaSO4 solution at a bias of 0.4 V vs RHE) was obtained under a simulated solar light.

4.4. Finite element method simulation (FEM)

CST Microwave Studio (version 2016) was used for FEM Solution. The 3D simulation model was designed as a simplified heterostructure with Al particles in BTO. The incident laser wavelength was set at 500 nm with the polarization direction along the z-axis. The electric field distributions of the hybrid nanocavity arrays were monitored across the middle of the BTO nanocavity in the x-y planes.

4.5. Hydrogenation of 4-nitrophenol

To investigate the photocatalytic performance for hydrogenation of 4-nitrophenol (4-NP), the heterostructure foams with a size of 4 cm^{-2} were added into 50 mL of aqueous solution containing 2 mmol $NaBH_4$ and 0.02 mmol 4-NP. The reactor was excited by a solar light simulator or both solar light and magnetic vibration. During the solar light irradiation, the suspension was mechanically stirred with a very slow rotation speed to establish a uniform concentration of the solution. To monitor the reaction, 3 mL mixture were removed to a microscale quartz cuvette every 5 min and the UV–vis absorption spectra were measured immediately. The concentrations of 4-NP were calibrate by the absorption peaks at 400 nm.

Acknowledgements

This work is financially supported by the National Natural Science Foundation of China (Grant No. 61774020, 51672148, 51272123, 51802021). Science and Technology Plan of Shenzhen City (Grant No. JCYJ20180306173235924), Fund of IPOC BUPT (Grant No. IPOC2017ZT06, 2019RC22) and Fundamental Research Funds for the Central Universities (Grant No. 2018XKJC05, 505019116), China. This work is also financially supported by the National Key Research and Development Program of China (2016YFA0202703), the “Hundred Talents Program” of the Chinese Academy of Science and State key laboratory of precision measuring technology and instruments (Tianjin University).

Appendix A. Supplementary data

Supplementary data to this article can be found online at https://doi.org/10.1016/j.nanoen.2019.05.067.

References

[1] A. Polman, K.R. Catchpole, Opt. Express 16 (2008) 21793.
[2] X. Zhang, Y.L. Chen, R.S. Liu, D.P. Tsai, Rep. Prog. Phys. 76 (2013) 046401.
[3] L. Guo, Z. Yang, K. Marcus, Z. Li, B. Luo, L. Zhou, X. Wang, Y. Du, Y. Yang, Energy Environ. Sci. 11 (2017) 106–114.
[4] N.T. Nguyen, M. Altomare, J. Yoo, P. Schmuki, Adv. Mater. 27 (2015) 32083215.
[5] L. Shi, W. Zhou, Z. Li, S. koul, A. Kushima, Y. Yang, ACS Nano 12 (2018) 6335–6342.
[6] L. Wang, S. Liu, Z. Wang, Y. Zhou, Y. Qin, Z.L. Wang, ACS Nano 10 (2016) 2636–2643.
[7] S. Lin, X.P. Bai, H.Y. Wang, H.L. Wang, J.N. Song, K. Huang, C. Wang, N. Wang, B. Li, M. Lei, H. Wu, Adv. Mater 29 (2017) 1703238.
[8] H. Wang, R.P. Liu, Y.T. Li, X.J. Lü, Q. Wang, S.Q. Zhao, K.J. Yuan, Z.M. Cui, X. Li, S. Xin, R. Zhang, M. Lei, Z.Q. Lin, Joule 2 (2018) 337–348.
[9] L. Guo, K. Liang, K. Marcus, Z. Li, L. Zhou, P.D. Mani, H. Chen, C. Shen, Y. Dong, L. Zhai, Y. Yang, ACS Appl. Mater. Inter. 8 (2016) 34970–34977.
[10] C.L. Bianchi, P. Canton, N. Dimitratos, F. Porta, L. Prati, Catal. Today 102 (2005) 203–212.
[11] R.G. Quhe, J.C. Liu, J.X. Wu, J. Yang, Y.Y. Wang, Q.H. Li, T.R. Li, J.B. Yang, H.L. Peng, M. Lei, J. Lu, Nanoscale 11 (2019) 532–540.
[12] A. Agrawal, S.H. Cho, O. Zandi, S. Ghosh, R.W. Johns, D.J. Milliron, Chem. Rev. 118 (2018) 3121–3207.
[13] X.T. Wang, Y. Cui, T. Li, M. Lei, J.B. Li, Z.M. Wei, Adv. Opt. Mater. 3 (2019) 1801274.
[14] J.H. Lin, Y.H. Tsao, M.H. Wu, T.M. Chou, Z.H. Lin, J.M. Wu, Nano Energy 31 (2017) 575–581.
[15] L.J. Zhang, S. Li, B.K. Liu, D.J. Wang, T.F. Xie, ACS Catal. 4 (2014) 3724–3729.
[16] Z. Li, L. Shi, D. Franklin, S. Koul, A. Kushima, Y. Yang, Nano Energy 51 (2018) 400–407.

[17] D. Gérard, S.K. Gray, J. Phys. D Appl. Phys. 48 (2014) 184001.
[18] D. Gerard, S.K. Gray, Phys. Rev. 6 (1972) 4370–4379.
[19] H.D. Li, Y.H. Sang, S.J. Chang, X. Huang, Y. Zhang, R.S. Yang, H.D. Jiang, H. Liu, Z.L. Wang, Nano Lett. 15 (2015) 2372–2379.
[20] K. Bi, M.H. Bi, Y.N. Hao, W. Luo, Z.M. Cai, X.H. Wang, Y.H. Huang, Nano Energy 51 (2018) 513–523.
[21] Z.L. Wang, J. Song, Science 312 (2006) 242–246.
[22] W. Wu, L. Wang, Y. Li, F. Zhang, L. Lin, S. Niu, D. Chenet, X. Zhang, Y. Hao, T.F. Heinz, J. Hone, Z.L. Wang, Nature 514 (2014) 470–474.
[23] Y.L. Liu, J.M. Wu, Nano Energy 56 (2019) 74–81.
[24] J. Wang, Y. Chen, L.-A. Kong, Y. Fu, Y. Gao, J. Sun, Appl. Phys. Lett. 113 (2018) 151101.
[25] W. Wu, X. Wen, Z.L. Wang, Science 340 (2013) 952–957.
[26] J. Zhao, Z. Wei, Q. Zhang, H. Yu, S. Wang, X. Yang, G. Gao, S. Qin, G. Zhang, Q. Sun, Z.L. Wang, ACS Nano 13 (2019) 582–590.
[27] Q. Sun, W. Seung, B.J. Kim, S. Seo, S.W. Kim, J.H. Cho, Adv. Mater. 27 (2015) 3411–3416.
[28] W. Wu, Z.L. Wang, Nat. Rev. Mater. 24 (2016) 16031.
[29] Z.L. Wang, W. Wu, C. Falconi, MRS Bull. 43 (2018) 922–927.
[30] Q. Sun, D.H. Ho, Y. Choi, C. Pan, D.H. Kim, Z.L. Wang, J.H. Cho, ACS Nano 10 (2016) 11037–11043.
[31] S. Kim, Y.J. Choi, H.J. Woo, Q. Sun, S. Lee, M.S. Kang, Y.J. Song, Z.L. Wang, J.H. Cho, Nano Energy 50 (2018) 598–605.
[32] Y. Chen, G. Gao, J. Zhao, H. Zhang, J. Yu, X. Yang, Q. Zhang, W. Zhang, S. Xu, Y. Meng, Q. Sun, Adv. Funct. Mater. (2019) 201900959.
[33] J. Sun, Fu Y. Fu, Q. Wan, J. Phys. D Appl. Phys. 51 (2018) 314004.
[34] L. Zhao, Y. Zhang, F. Wang, S. Hu, X. Wang, B. Ma, H. Liu, Z.L. Wang, Y. Sang, Nano Energy 39 (2017) 461–469.
[35] M.H. Wu, J.T. Lee, J.C. Yun, M. Srinivaas, J.M. Wu, Nano Energy 40 (2017) 369–375.
[36] S. Xu, L. Guo, Q. Sun, Z.L. Wang, Adv. Funct. Mater. 29 (2019) 1808737.
[37] L. Guo, Q. Sun, K. Marcus, Y. Hao, J. Deng, K. Bi, Y. Yang, J. Mater. Chem. A 6 (2018) 22005.
[38] X.M. Li, M.H. Bi, L. Cui, Y.Z. Zhou, X.W. Du, S.Z. Qiao, J. Yang, Adv. Funct. Mater. 27 (2017) 1605703.
[39] M.W. Knight, L. Liu, Y. Wang, L. Brown, S. Mukherjee, N.S. King, H.O. Everitt, P. Nordlander, N.J. Halas, Nano Lett. 12 (2012) 6000–6004.
[40] H. He, J. Lin, W. Fu, X. Wang, H. Wang, Q. Zeng, Q. Gu, Y. Li, C. Yan, B.K. Tay, Adv. Energy Mater. 14 (2016) 1600464.
[41] S. Sandip, P. Anjali, K. Subrata, B. Soumen, P. Tarasankar, Langmuir 26 (2010) 2885–2893.
[42] B. Bharat, G.J. Gabriel, M.J. Akbashev, M.E. Booher, Langmuir 29 (2013) 4225–4234.

Limin Guo received her Ph. D. from Tsinghua University in 2013. She is now an assistant professor in Beijing University of Posts and Telecommunications. Her research interest is focused on highly ordered nanoscaled semiconductor materials or 2D materials and their application in energy conversion and storage, like photocatalysis, solar cell, fuel cells.

Caifu Zhong received his Ph. D. from Tsinghua University in 2012. He is now an associate researcher in Chinese Academy of Macroeconomic Research, National Development and Reform Commission. He is mainly focus on the research of renewable energy, especially solar cell, energy storage systems, hydrogen energy.

Jinqing Cao received his B.Eng. from Nanjing University of Aeronautics and Astronautics in 2018. He is now a postgraduate in Beijing University of Posts and Telecommunications. His research interest is focused on nano scaled perovskite materials and their application in photoelectrocatalysis, information functional materials.

Yanan Hao received her Ph. D. from Tsinghua University in 2016. She is now an associate researcher in Beijing University of Posts and Telecommunications. Her research interest is focused on nano scaled perovskite materials and their application in microelectronics and energy storage, information functional materials and devices.

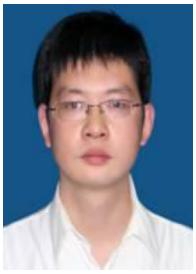

Ming Lei received his Ph.D. from Institute of physics, Chinese academy of science in 2007. From 2007 to 2008, he worked as a postdoctor in The Hong Kong University of Science and Technology and Chinese University of Hong Kong. He is now a distinguished professor in Beijing University of Posts and Telecommunications. His research group focuses on nanostructured materials and devices for photoelectric conversion and photocatalysis.

Ke Bi received his Ph. D. from Nanjing University of Aeronautics and Astronautics in 2012. From 2012 to 2014, he worked as an assistant researcher in Tsinghua University. He is now an associate professor in Beijing University of Posts and Telecommunications. His research group focuses on information functional ceramics and devices, metamaterials, microwave devices such as antennas and filters.

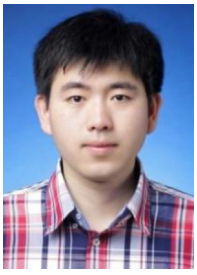

Prof. Qijun Sun received his Ph. D from Gachon University in 2013. After that, he worked as a postdoctoral researcher in POSTECH (2013) and SKKU (2014). In 2015, he worked in Sungkyunkwan University as a research professor. From 2016, he joined Beijing Institute of Nanoenergy and Nanosystems (Chinese Academy of Sciences), as the principal investigator of Functional Soft Electronics Lab. The Main research interests of his group include graphene device based E-skin, organic electronic device, graphene electronics, printing electronics, micro-nano fabrication and transparent conducting films, aim to develop advanced systems for human health monitoring and human-machine interface.

Prof. Zhong Lin Wang received his Ph.D. from Arizona State University in physics. He now is the Hightower Chair in Materials Science and Engineering, Regents' Professor, Engineering Distinguished Professor and Director, Center for Nanostructure Characterization, at Georgia Tech. Dr. Wang has made original and innovative contributions to the synthesis, discovery, characterization and understanding of fundamental physical properties of oxide nanobelts and nanowires, as well as applications of nanowires in energy sciences, electronics, optoelectronics and biological science. His discovery and breakthroughs in developing nanogenerators established the principle and technological road map for harvesting mechanical energy from environment and biological systems for powering a personal electronics. His research on selfpowered nanosystems has inspired the worldwide effort in academia and industry for studying energy for micro-nano-systems, which is now a distinct disciplinary in energy research and future sensor networks. He coined and pioneered the field of piezotronics and piezophototronics by introducing piezoelectric potential gated charge transport process in fabricating new electronic and optoelectronic devices. Details can be found at: www.nanoscience.gatech.edu.